Lab report
K223 Nuclear γ-γ Angular Correlations

Chenhuan Wang and Harilal Bhattarai

September 1, 2020

In this experiment, we investigate nuclear properties of cobalt nuclei via angular correlation. Number of coincidence is measured in dependence on angle between two photons. There is strong anisotropy present. The measured data are fitted with the theoretical prediction function of 420 cascade and calculated the angular correlation coefficients: $A_{22} = 0.0849 \pm 0.0057$ and $A_{44} = -0.0002 \pm 0.0063$. Closer investigation reveals that measured values differ from theoretical prediction by 4σ. Despite this, other types of cascade are excluded almost 100%.

1 Introduction

Angular correlation from cascades can appear because of the unequal spin states distribution in the intermediate states. By choosing one photon from cascades one puts constraints in angular distribution of second photon [1]. For detection of gamma rays, scintillator and photomultiplier are used. In order to extract both energy and timing accurately, so-called "fast-slow principle" is used. The main parts of the experiment are setting up the experiment and investigating nuclear properties of ^{60}Co via angular correlation of γ-γ cascades [1].

Section 2 briefly talks about theories underlying angular correlation of cascades. Section 3 explains functionality of electronics used in setup. Tasks for preparation are in section 4. In section 5, one can find calibration and preparation processes. Data analysis is presented in section 6. Conclusion is in section 7

2 Theory

Angular correlation of gamma rays of multipole moments $L_{1,2}$ from γ-γ cascade $I_i \rightarrow I \rightarrow I_f$ is defined as

$$W(\theta) = 1 + \sum_{k=2,\text{ even}}^{k_{\max}} A_{kk} P_k(\cos\theta) \tag{1}$$

with A_{kk} (known given the information of nucleus) coefficients, $P_k(\cos\theta)$ the Legendre polynomials, and $k_{\max} = \min(2I, 2L_1, 2L_2)$[2]. Alternatively, equivalent definition is sometimes used [3]

$$W(\theta) = 1 + \sum_{1}^{l} a_i \cos^{2i}\theta \tag{2}$$

Coefficient A_{kk} is determined, generally with mixed multipole components L'_n and L_n ($n = 1, 2$), by

$$A_{kk} = A_k(L_1 L'_1 I_i I) A_k(L_2 L'_2 I_f I) \tag{3}$$

$$A_k(L_n L'_n I_{i,f} I) = \frac{F_k(L_n L_n I_{i,f} I) + 2\delta_1(\gamma) F_k(L_n L'_n I_{i,f} I) + \delta_1^2(\gamma) F_k(L'_n L'_n I_{i,f} I)}{1 + \delta_1^2(\gamma)} \tag{4}$$

$$F_k(LL'I'I) = (-1)^{I'+I-1} \left[(2L+1)(2L'+1)(2I+1)(2k+1)\right]^{1/2}$$
$$\times \begin{pmatrix} L & L' & k \\ 1 & -1 & 0 \end{pmatrix} \begin{Bmatrix} L & L' & k \\ I & I & I' \end{Bmatrix} \tag{5}$$

$$\delta_1(\gamma) = \frac{\langle I|L'_1 \pi'_1|I_{i,f}\rangle}{\langle I|L_1 \pi_1|I_{i,f}\rangle} \tag{6}$$

with round brackets being $3j$-symbols and curly brackets $6j$-symbols[2]. Their value can be easily found tabulated, e.g. in [4] and [5]. $\delta_n(\gamma)$ quantifies the mixing of two multipole moments and should be determined by some other methods. If we assume $L'_n = L_n + 1$ (this is reasonable because of selection rules), then there are 7 quantum numbers to nail down the coefficients: $I_i, I, I_f, \delta_{1,2}, L_{1,2}$[2].

Example with $0 \to 1 \to 0$ γ-γ cascade. Since the first and last states are of spin 0, the multipolarities of emitted photon must be 1, thus dipole-dipole radiation. According to [3]

$$W(\theta) = 1 + \cos^2(\theta) \tag{7}$$

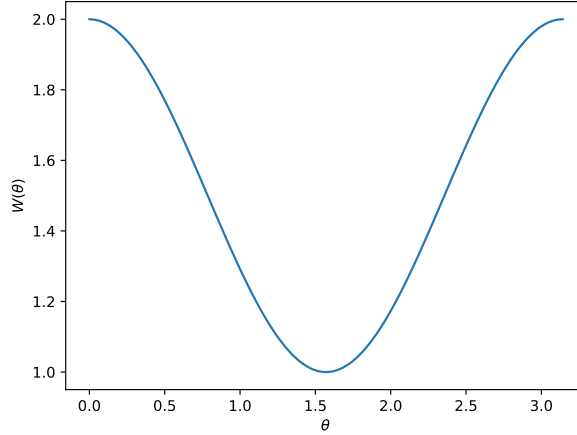Plot of this angular correlation can be found in figure 1.

Figure 1: Angular correlation of hypothetical 010 cascade

Hyperfine structure can have influence on the angular correlation, since with quantization axis along the direction of first photon the first photon will cause transitions among the m-states. Thus in the end, the direction of second photon is altered. The perturbed angular correlation is given as

$$W(k_1, k_2, t) = \sum_{m_i, m_f, m_a, m'_a} \langle m_f|H_2\Lambda(t)|m_a\rangle \langle m_a|H_1|m_i\rangle \langle m_f|H_2\Lambda(t)|m'_a\rangle^* \langle m'_a|H_1|m_i\rangle^* \tag{8}$$

2

where $H_{1,2}$ represents the interaction between nucleus and radiation field and $\Lambda(t)$ is an unitary operator describing influence of extranuclear perturbation. k_1 and k_2 are wave vector of photons. [2].

Information can be obtained from measurement of γ-γ angular correlations (without extranuclear perturbation): spin angular momenta of excited states, the multipole orders, and the relative multipole composition of radiative transitions[6]. With extranuclear perturbation, we can in addition extract g-factor and quadrupole momentum of intermediate state. Internal fields of solids, liquids, and metal crystals can be investigated. And some changes in atomic shell is possible to study [2].

3 Experimental setups

3.1 Key components

Scintillation detector detects ionizing radiation in general. Here only gamma radiation is relevant. The purpose of scintillator is to lower photon energy via photoelectric effect, Compton scattering, and pair production [7]. It is then connected to photomultiplier tube (PMT) to generate signals.
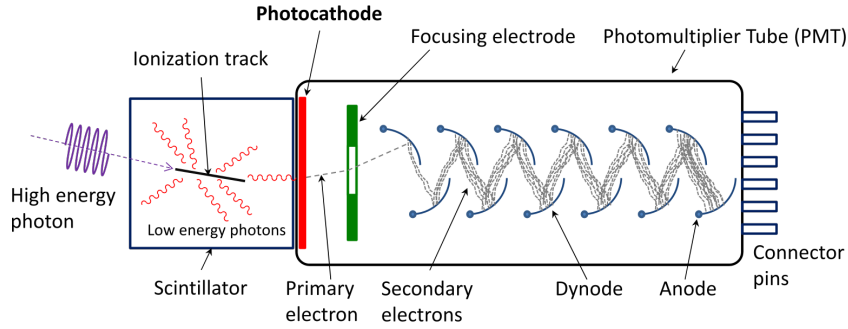

Figure 2: Scintillator with PMT [8]

Fast-slow coincidence is the technique to measure the ionizing radiation separately. The "slow" part will determine the energy of incoming radiation. And the "fast" part is used to measure the time as precisely as possible, since the photomultiplier will be brought to saturation and the height of the pulse is not proportional to radiation energy any more [9].

SCA stands for single channel analyzer. Basically it is advanced version of simple discriminator, as one can set both upper-level (ULD) and lower-level discriminator (LLD) for SCA. It reads the input pulse and check whether it is within the preset limits or not. If it is, SCA will produce a uniform digital signal. When applied to PMT, the height of pulse corresponds to energy of radiation. If SCA is built in after PMT, we are essentially picking out photons within the SCA window. Thus the name [10].
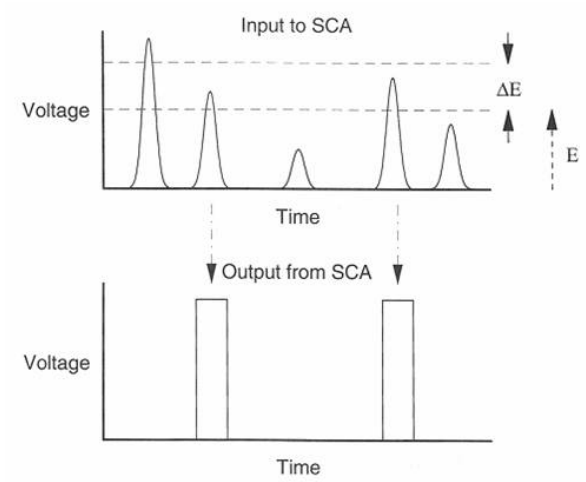
Figure 3: Single Channel Analyzer [8]

CFD stands for constant fraction discriminator. As its name suggests, it gets triggered at some preset fraction of maximal amplitude, in order to reduce "walk". In simplest form, CFD works by splitting input signals, inverting one of them, and adding delay to the other. In the end, by combining these two together, we get logic signal with minimal walk [11].

Expected Spectrum of ^{60}Co would predominantly consists of $0.31\,\text{MeV}$ β-line and $1.1732\,\text{MeV}$, $1.3325\,\text{MeV}$ γ-line [12]. Its γ-spectrum can be found in 4, where one can see two clear peaks corresponding to the γ-radiations and some background because of various effects, like pair production (higher E), Compton scattering (mid E), and photoelectric effect (low E) [7].
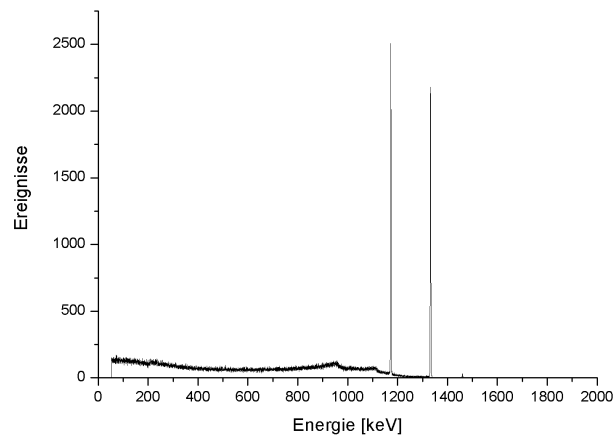

Figure 4: ^{60}Co γ-specturm [13]

4 Task for preparation

4.1 Which distances to pick?

Obviously, the count (rate) should be proportional to the solid angle ignoring the anisotropy of radiation. This assumption should not bring too much influence to the results, as long as the size of detection is accounted for in final analysis as (systematic) error. In [2], true count rate is given by

$$N_i^t(\theta) = M p_i \Omega_i \epsilon_i \tag{9}$$

with M the number of nuclear integrations per uni time, p_i the probability that this integration is selected, Ω_i is solid angle in unit 4π, and ϵ_i the detector efficiency. According to formula of solid angle, it means that

$$N_i^t(\theta) \propto \frac{1}{r_i^2} \tag{10}$$

Follow the same principle, true number of coincidence can be written as [2]

$$C^t(\theta) = M p_1 p_2 \Omega_1 \epsilon_1 \Omega_2 \epsilon_2 \epsilon_c K(\theta) \tag{11}$$

where ϵ_c is the efficiency of coincidence unit and $K(\theta)$ is the directional correlation function. $K(\theta)$ is basically the "measured" version of $W(\theta)$, i.e. what we have in the real world. The coincidence rate is then $C^t(\theta)/N_1^t(\theta)$ thus

$$\frac{C^t(\theta)}{N_1^t(\theta)} \propto \frac{1}{r_2^2} \tag{12}$$

The angular "asymmetry" is represented as the coefficients A_{kk}. With correction factor, we write

$$A_{kk} = \frac{A_{kk}^{\mathrm{exp}}}{Q_{kk}} \tag{13}$$

And it can be calculated by [2]

$$Q_{kk} = Q_k(1) Q_k(2) \tag{14}$$

$$Q_k(i) = \frac{J_k(i)}{J_0(i)} \tag{15}$$

$$J_k(i) = \int_0^{\pi/2} \epsilon_i(E, \alpha) P_k(\cos\alpha) \sin\alpha \, \mathrm{d}\alpha \tag{16}$$

$$\epsilon(E, \alpha) = 1 - \exp\{-\tau(E) X(\alpha)\} \tag{17}$$

with $\tau(E)$ the total absorption coefficient and $X(\alpha)$ the distance traversed in the crystal.

The correction factor will certainly affect the error of angular correlation function, multiplicatively to be specific.

According to table in [2], $h = 10\,\mathrm{cm}$ would provide the most precise measurement, since the Q_i's are closer to 1. So in the actual experiment, one can try to measure the event rate in a short time period. Then the distance should be so chosen that enough data will be taken in the given time but still have maximal precision.

4.2 Which angles to pick?

The angular correlation function is given in the form of [1]

$$f(\theta) = A(1 + B\cos^2\theta + C\cos^4\theta) \tag{18}$$

It can be rewritten with $\alpha = B + C$ and $\beta = B - C$,

$$f(\theta) = A\left(1 + \frac{\alpha + \beta}{2}\cos^2\theta + \frac{\alpha - \beta}{2}\cos^4\theta\right) \tag{19}$$

Predicted values for A_{22} and A_{44} without mixing are given in [2]. Then the predicted correlation function is

$$\begin{aligned}
W(\theta) &= 1 - \frac{A_{22}}{2} + \frac{3}{8}A_{44} + \left(\frac{3}{2}A_{22} - \frac{15}{4}A_{44}\right)\cos^2\theta + \frac{35}{8}A_{44}\cos^4\theta \\
&= 0.952412 + 0.118875\cos^2\theta + 0.039813\cos^4\theta
\end{aligned} \tag{20}$$

Need to "scale" it, so that 0.9524 gets absorbed in A. Then we have

$$B = 0.124815, C = 0.041802$$

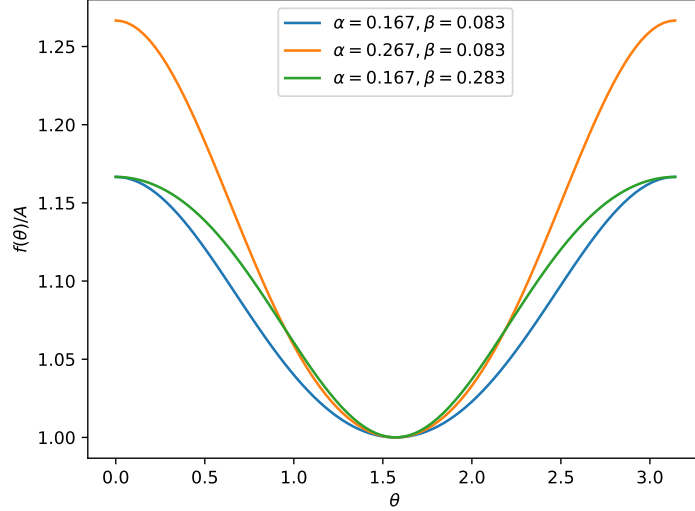Plot correlation with these two coefficients with slight variation, we have figure. 5 From it,

Figure 5: Correlation with different α and β

it is clear that to determine α, we need in principle only one point ($\theta = 0$ or $\theta = \pi$). But determination of β requires small increments in angle between 0 and $\pi/2$.

4.3 How to correct for de-adjustment?

In actual setup, the source might not lie perfectly in the center of circle of detectors. It will certainly cause a distortion in data, since extra "angular correlation" will be introduced. Depending on in which direction the source is off from the center of circle, the angular correlation could have an obvious asymmetry or just simply gets stretched out. To correct this, count rates of two detectors needs to be recorded. Coincidence rate should be normalized against these count rates.

5 Experimental procedure

In this experiment, we set up two detectors with equidistant from the source. Distance from detector to source is $5\,cm$ for both detectors, as suggested by tutor. This ensures precision within the limited time frame.

Fast and slow signals circuits are separate readout from detectors. Both of them get combined in to an universal counter (UC) through a gate and delay $(G^2 - D^2)$. Two CFDs are connected to filter out zero crossing in fast signal circuit and two amplifiers are connected in slow signal circuit. Three delays are used, two in slow signal circuit (built-in in SCA) and one between CFD2 and FC. A timer connected with all counters to fixed the counting time. The figure 6 shows a schematic of the set and the tasks we did on this experiment are described in the following. Detector part in real life is shown in 7.

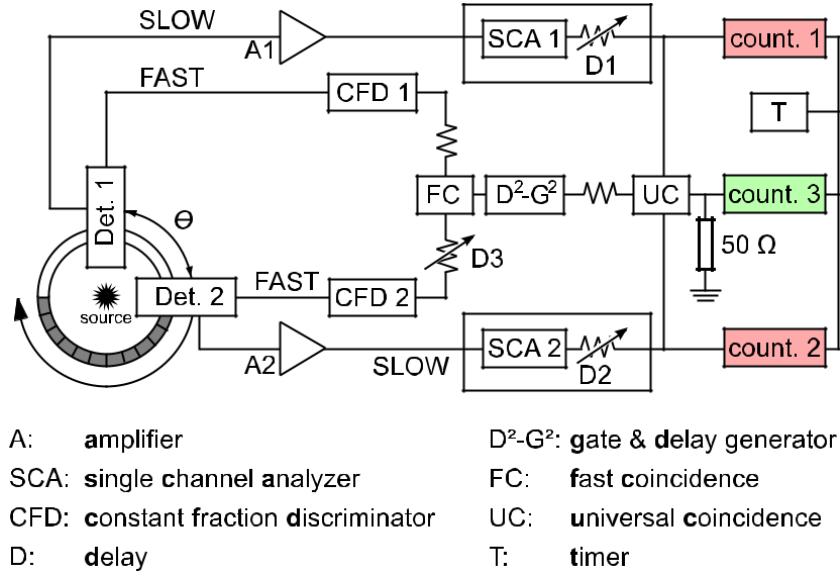| A: | amplifier | D²-G²: | gate & delay generator |
SCA:	single channel analyzer	FC:	fast coincidence
CFD:	constant fraction discriminator	UC:	universal coincidence
D:	delay	T:	timer

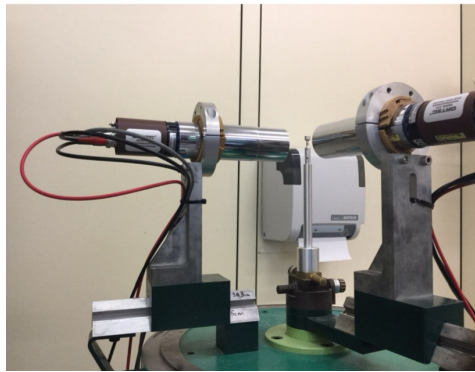Figure 6: Set up of fast and slow coincidence circuit [1].

Figure 7: Set up of two detectors where one is fixed and another one is movable to rotate at a fixed radial distance from the fixed detector.

5.1 Adjusting the gain of the Amplifier

First, we adjusted the gain of both amplifiers (A_1 and A_2) during the set up of the experiment. The amplifiers output is linear up to $V_{\max} = 9\,\mathrm{V}$. With oscilloscope the amplifications of amplifiers are set to obtain a signal without saturation. Here we took gains of the amplifiers as much as possible. Signals get saturated if signals have a clear plateau.
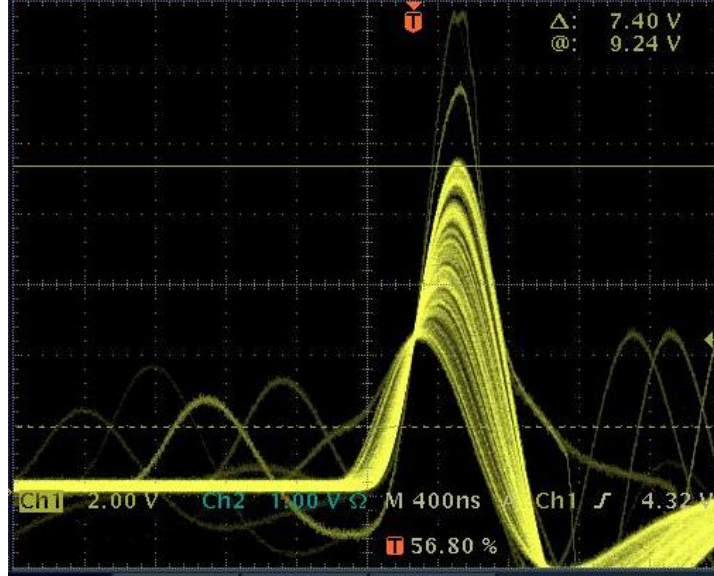

Figure 8: Amplified signal output from the detector. The other output looks the same.
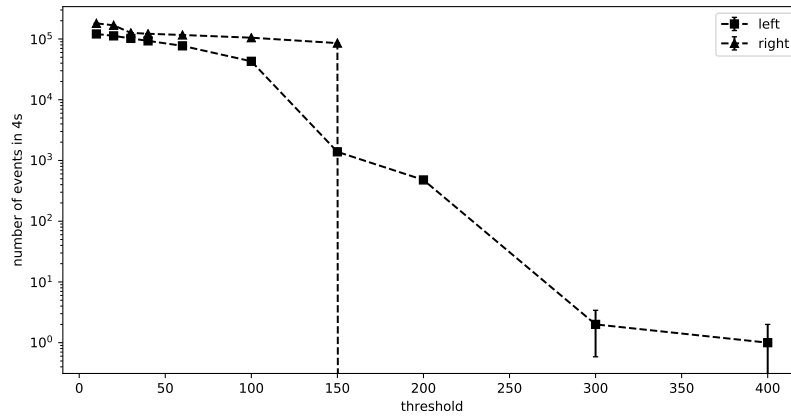
5.2 Adjusting of the CFD

Figure 9: Number of events with source. Note vertical axis used log-scale.

CFD has a threshold-discriminator which helps to filter out zero crossing that belongs to electronic noise and not to a true scintillation signal [1]. Performing a threshold scan allows
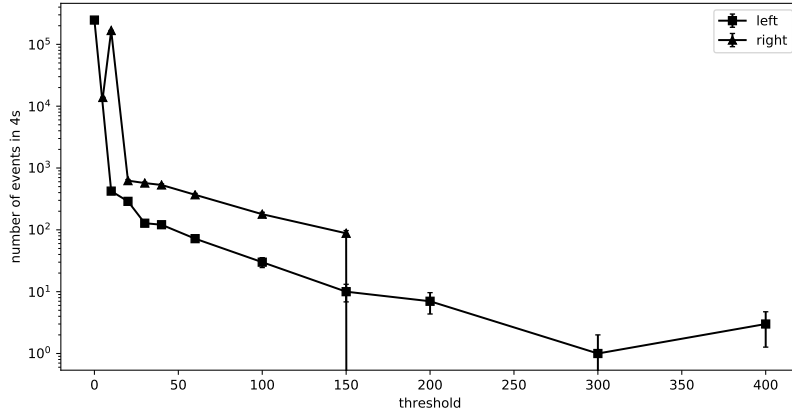
Figure 10: Number of events without source. Note vertical axis used log-scale.

to search out the right compromise. For that, CFD has restriction upon the minimum and maximum signals.

Thresholds of CFD should be adjusted to detect only true signals, not the background noise signals. In that step, the negative outputs of the both CFDs are connected to the counters and the events are counted with and without source. Figure 9 and 10, respectively, show the number of events with and without inserting source. Errors are calculated with $\Delta N \approx \sqrt{N}$.

Number of events without source contain only random events, aka backgrounds. With source it contains both signals and backgrounds. Figure 9 has quite drastic drop in number of events, whereas in figure 10 the drop is rather continuous after 30 or so. In the end, we set the threshold to 30, since most random events are cut and wanted signals are still basically untouched.

5.3 Setting up the Fast Coincidence

Here we want to make sure that true coincidences arrive at same time (within resolving time of coincidence unit, to be precise). First, we connected both CFDs to the oscilloscope and triggered on the first channel signals. Then, on the second channel, true coincidence pulses are concentrated in small region. The random events are not the events we are looking for.

We inserted a fixed delay into one of the fast branches and a variable delay into the other one, so that we can see the full prompt curve. Then, the CFDs are connected to the fast coincidence unit and the count rates are measured for different (variable) delay with resolving time 25 ns.
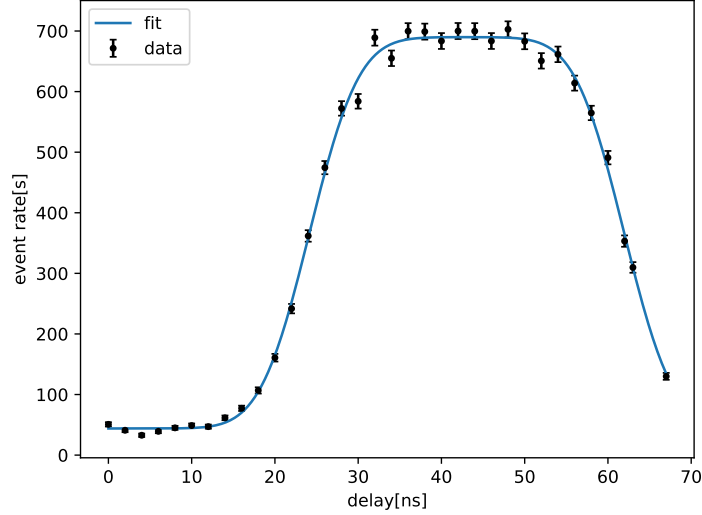
Figure 11: Prompt curve

Indeed, the prompt curve looks like a box with smeared egdges as stated in [1]. Data points are fitted wit function

$$f(t) = A_0 + A_1 \left(\frac{1}{2} + \mathrm{erf} \left(\frac{t - t_0}{\sigma} \right) \cdot \mathrm{erf} \left(\frac{t_1 - t}{\sigma} \right) \right) \tag{21}$$

This is reasonable considering that signals are gaussian. Data and fit curve can be found in figure 11.

These parameters each represent something physical of the experiment: A_0 random coincidence since with extreme low/high delay the true coincidences don't safisfy the conincidence criteria, A_1 related to source intensity and detector efficient, t_i resolution of corresponding detector, σ resolving time of coincidence unit. Thus the width of the plateau depends on σ. This can be easily understood as if we turn up the resolving time, then there will more events considered as coincidences. The slopes are related to detector (time) resolutions, since it smears the CFD's logic output timing. Parameters from fitting are

$$t_0 = (24.151 \pm 0.151)\,\mathrm{ns}$$
$$t_1 = (61.949 \pm 0.152)\,\mathrm{ns}$$
$$A_0 = (205.436 \pm 3.823)\,\mathrm{s}^{-1}$$
$$A_1 = (323.007 \pm 3.580)\,\mathrm{s}^{-1}$$
$$\sigma = (6.612 \pm 0.242)\,\mathrm{ns}$$

Correlations of parameters are quite small, since the off-diagonal entries of covariance matrix are at least one magnitude lower. Thus correlations are neglected.

Shape of the prompt curve will change to basically flat (constant count rate) if the resolving time is chosen too short or too long: either no signals will be picked up or every pair of inputs will be counted as coincidence.

5.4 Setting up the Slow Coincidence

Again timings of output of fast coincidence and two SCAs need to be aligned. SCAs have built-in delays. With oscilloscope, signals are properly aligned with leading edges. It often gives us maximal overlap as well. In figure 12 the peaks are correctly aligned with each other.
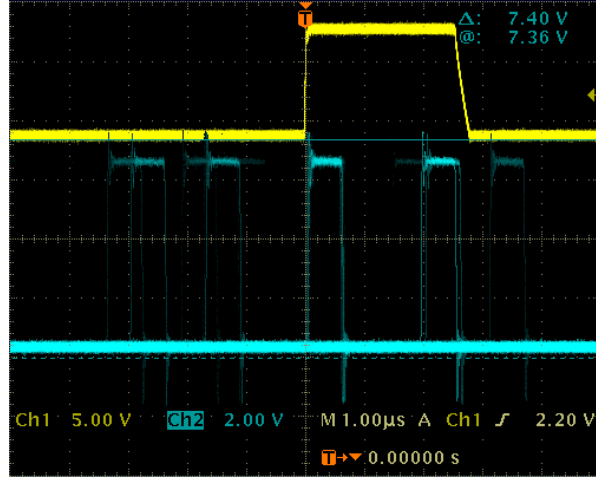

Figure 12: The timing alignment of signals from FC and two SCAs.

5.5 Calibrating the Signal Channel Analyzer

The SCAs are used to select the energy deposited in the detector. In this step, we performed the energy calibration and recorded the energy-spectrum by using SCAs. For that the SCAs are set to their window mode. Window size is kept constant due to normalization. We want to see all structures of energy spectrum, so 20 window width is selected.

For lower statistical error, events are counted until roughly 1% precision is reached. Figure 13 shows the energy spectra. Quite awful in this plot is that second peak of right signals doesn't appear. The SCA windows should be set to include both photopeaks for higher coincidence rate. So amplification of right slow circuit is lowered. Figure 14 shows energy spectra after we readjusted amplification. In the end, SCA windows are set to $[720, 960]$.

5.6 Main Measurement

After adjusting all the involving apparatus in the experiment, we stated to perform the main measurement of the experiment. The count rates are measured for different angles between these two detectors. We have taken firstly some measurements with larger steps and longer duration, then some measurements with smaller steps and shorter duration. Throughout whole experiment, measurement at 180° is repeated three times in order to have knowledge of setup stability and systematic errors.

In the end, an extra measurement of random coincidence is carried out, where the variable delay in fast branches is turned all the way up, so that true coincidences are not counted. The random coincidence rate is

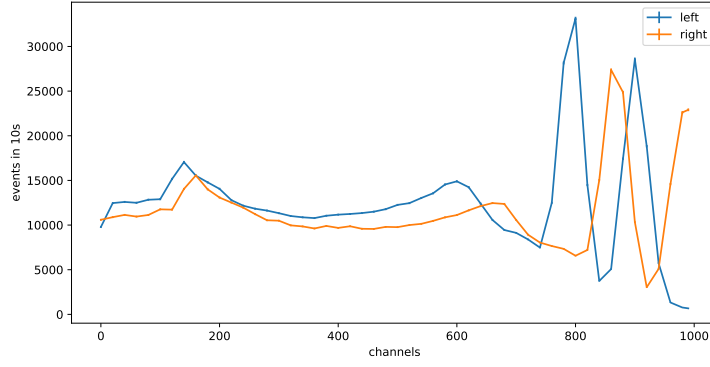$$\dot{R} = (2.218 \pm 0.061)\,\text{s}^{-1} \tag{22}$$
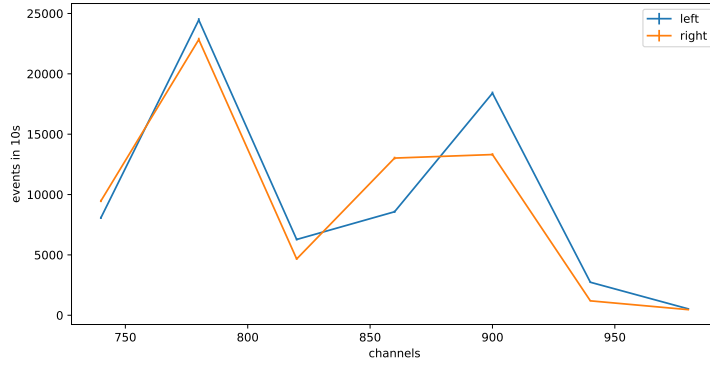
Figure 13: The energy spectra.

Figure 14: The energy spectra after readjusting amplification.

Delays of SCAs remain unchanged. This would not have big impact on measurement of random coincidence, since only fast circuit has accurate timing information.

Random coincidence rate can also be calculated. Assuming extremely narrow signal peak (but still can be seen by fast circuit) and uniformly distributed signals, random coincidence rate is then the rate of two signals falling within resolving time. It is given as [14]

$$\dot{R}_{\mathrm{pred}} = \dot{N}_1 \dot{N}_2 \Delta t = (1.643 \pm 0.013)\,\mathrm{s}^{-1} \tag{23}$$

Ideally the count rates are same for both detectors $\dot{N}_1 = \dot{N}_2$, but as we will see, there is misalignment. Count rates measured in main measurements are used here and their mean and standard deviation are calculation, since there are more than one set of data. Resolving time is again $\Delta t = 25\,\mathrm{ns}$. Errors are propagated properly.

This doesn't match measured value. It could imply that there some systematic error in electronics. But also the assumption could not be valid. Here we see that random coincidence, a source of background, is proportional to resolving time. In figure 11, the plateau is still quite long. In principle, the resolving time can still be lowered so that true coincidence doesn't get affected but random coincidence gets reduced.

12

6 Analysis

Firstly the data needs to be corrected because of random coincidences and misalignment of the setup. Random coincidence rate $\dot{R}$ in 22 is simply subtracted from the coincidence rate. In calculation of error of count rate, error of random coincidence is considered as well.

It is thought to be acceptable to just use one random coincidence rate for all angles, since it has no angular dependence. Effects of misalignment on random coincidence need to be considered. That is why the data get correction for misalignment after this step.

In figure. 15, one can see a clear asymmetry in count rate of the mobile detector. This can be easily explained by source not being in the center of the setup. True coincidence rate should be anti-proportional to count rates in figure. 15. Since measured angular correlation function is determined up to a proportional constant anyway, the normalization factor κ is chosen to be the fraction of count rate at smallest angle and count rate at respective angle.
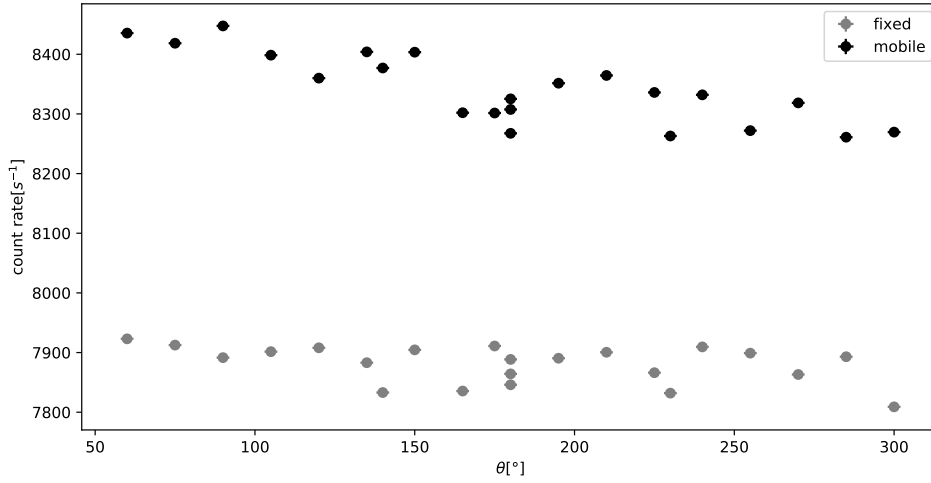

Figure 15: Raw count rate

Coincidence rates are normalized against the raw count rate with κ, in order to counter misalignment. True coincidence rate $\dot{C}_{\text{true}}$ is calculated via

$$\dot{C}_{\text{true}} = \kappa \cdot (\dot{C}_{\text{measured}} - \dot{R}) \tag{24}$$

During experiment, the setup and its environment might (inevitably) change, i.e. temperature. Measurements at 180° are repeated multiple times. Some variations have been seen. This introduces (one source of) systematic error and will be included in the further analysis.

$$\Delta\dot{C}_{\text{sys}} = 0.564 \tag{25}$$

Data after these corrections are plotted in figure. 16. Vertical error bars include statistical error and systematic error. Error of angle is estimated to be about 2 degrees.

A least squares fit of data using function in the form of (18) is carried out. Fitted function is drawn in blue in figure 16. Parameters are shown in table 4. One should emphasize that the errors in table 4 are only the diagonal entries of covariance matrix. There are still non-vanishing off-diagonal entries, i.e. variables are somehow correlated. This is the reason why
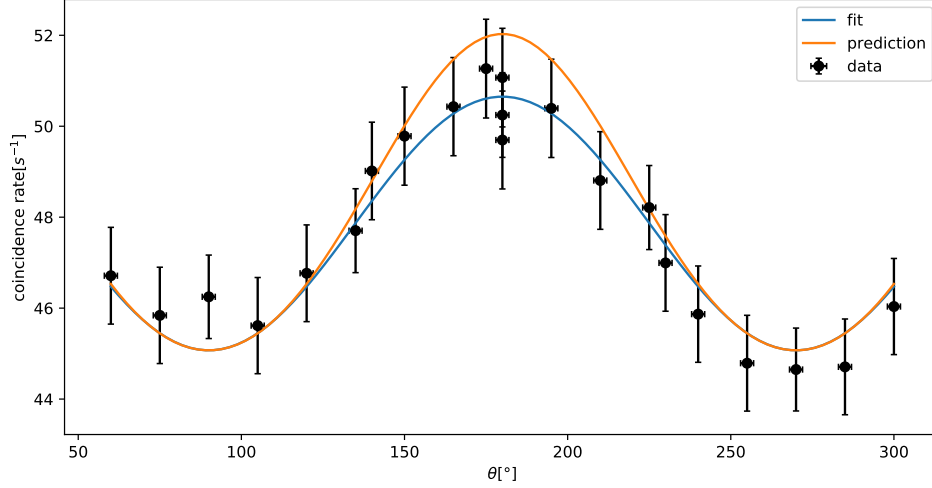
Figure 16: Angular correlation with fit and prediction

	fit	theory
A	45.0721 ± 0.2578	
B	0.1246 ± 0.0310	0.1213
C	-0.0008 ± 0.0289	0.0330

Table 1: Parameters of the curve shown in figure 16 and their theoretical values after being "corrected" for finite size of detector

drawing confidence intervals in figure 16 is not meaningful. Covariance matrix of these fitting parameters is

$$\Sigma_{ABC} = \begin{pmatrix} 0.066\,486\,01 & -0.006\,102\,61 & 0.004\,625\,04 \\ -0.006\,102\,61 & 0.000\,960\,16 & -0.000\,864\,38 \\ 0.004\,625\,04 & -0.000\,864\,38 & 0.000\,832\,77 \end{pmatrix} \tag{26}$$

Based on this value of A, we can plot the predicted function equation (20). Because of finite size of detector, prediction curve needs to be "corrected" by factor Q_k to correspond measured correlation curve. It is more convenient to apply this correction to fit curve than data points. Values of Q_k are taken from [2] with distance to source $h = 5\,\text{cm}$. Energy of γ-radiation in experiment is between $1\,\text{MeV}$ and $1.5\,\text{MeV}$ and only photopeaks are relevant. For convenience, mean values of Q_k of these two energies are used in calculation

$$Q_2 = 0.934, \ Q_4 = 0.792$$

Theoretical prediction with Q correction of fit parameters are also added in table 4.

It seems that prediction and measurement have at least OK agreement, only some deviation around 180° is present. But a closer look is necessary, since the fit parameters are correlated. For simplicity, we say that A has no correlation to other parameters and only its best-fit value is used. This will underestimate "distance" between theory and measurement. Taking only B and C components of equation (26), one can draw confidence intervals on parameter plane. In
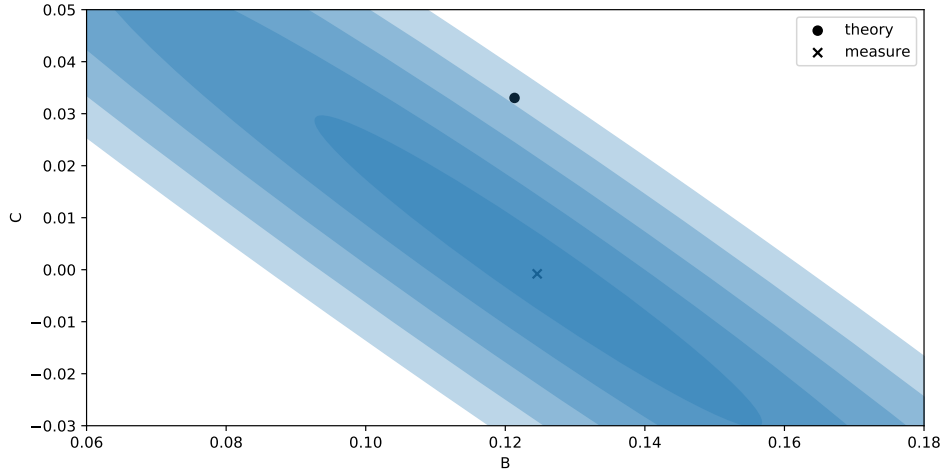
Figure 17: Regions on the plane (B, C) measured by experiment. Best-fit and theoretical prediction are included. The contours corresponds to 1σ, 2σ, 3σ, 4σ, 5σ confidence intervals.

figure 17, one can see prediction value lie roughly 4σ away from best-fit value, even though table 4 gives us roughly 1σ accuracy.

Just as a consistency check and to better understand origin of deviation, B and C can be converted into α, β like before.

$$\begin{pmatrix} \alpha \\ \beta \end{pmatrix} = \begin{pmatrix} 1 & 1 \\ 1 & -1 \end{pmatrix} \begin{pmatrix} B \\ C \end{pmatrix} \tag{27}$$

	fit	theory
α	0.1238	0.1544
β	0.1254	0.0883

Table 2: Prediction and measurement of α, β. Here theoretical value has been corrected by Q-factor.

Results are in table 2. Their covariance matrix is

$$\Sigma_{\alpha\beta} = \begin{pmatrix} 6.416\,647\,49 \times 10^{-5} & 1.273\,956\,76 \times 10^{-4} \\ 1.273\,956\,76 \times 10^{-4} & 3.521\,699\,20 \times 10^{-3} \end{pmatrix}$$

Thus deviations are present at all angles, not e.g. only around 180° when only α is off.

There is quite obvious asymmetry (with respect to 180°) present in the angular correlation. Ideally, this should not be in data, or at least after being corrected by considering misalignment. To better see the difference, data points are plotted in figure. 18. From this, we can see that the asymmetry can be well explained by the errors.

They need to be converted to A_{kk} coefficients and then corrected for finite size of detectors. As written in equation (20), both A_{22} and A_{44} decides the values of B and C (need to scale
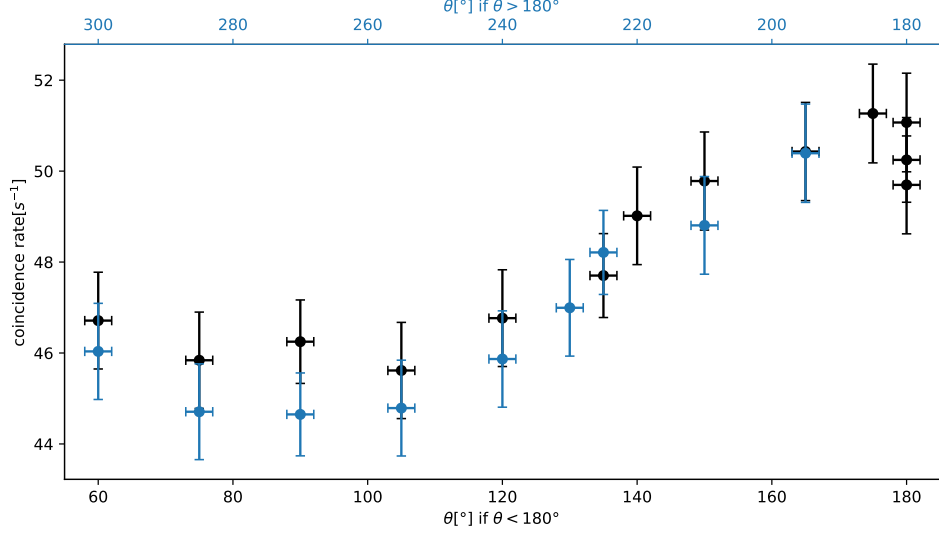
15

Figure 18: Angular correlation to see asymmetry. Color of data points correspond to the color of axis to use.

it, so that the constant term is unity!). Thus it involves finding the inverse of the matrix. The errors here are given without correlation considered, i.e. these are only diagonal entries of covariance matrix.

	fit with correction	theory
A_{22}	0.0849 ± 0.0057	0.1020
A_{44}	-0.0002 ± 0.0063	0.0091

Table 3: Measured coefficients after corrected for finite size of detectors and theoretical values

Fitting of angular correlation could also help us to exclude other cascades. From previous found values of B and C, one can conclude that 020, 121, 220, and 320 cascades are pretty much 100% excluded using coefficients provided by [3]. Alternatively, fit function can also only contain $\cos^2 \theta$ term. This fit curve visually doesn't differ from the previous curve visually, as expected since C from previous fit is almost vanishing. New fit parameters are Comparing this

	fit
A	45.0765 ± 0.1969
B	0.1237 ± 0.0077

Table 4: Parameters using alternative fit function. Errors are just the diagonal entries of covariance matrix.

B to values give in [3], the closest (positive) value is of 210 and 220 cascades with $B = 3/7 \approx 0.43$. Although Q correction is not included, we know for sure $Q \sim 1$, and measured value is no way near 0.43 (more than dozens of σs away). Some negative values are numerically closer

16

to measured value. But from the plot, coefficient B is obviously positive. We can say for sure, measured angular correlation does not correspond to any other cascades listed in [3].

7 Conclusion

In this experiment, we measured angular correlation between two photons emitted from ^{60}Co. Then, the data gets fitted with the theoretical prediction function and the angular correlation coefficients are calculated: $A_{22} = 0.0849 \pm 0.0057$ and $A_{44} = -0.0002 \pm 0.0063$. The non-zero values of these two angular correlation coefficients provide strong evidence for an angular correlation between two gamma rays emitted in 420 cascade of ^{60}Co. Via curve fitting, we can conclude that other types of cascade (020,121, 220, and 320) are basically 100% excluded.

Further investigation reveals that measured values differ from prediction by 4σ due to unknown systematic errors in the setup. One of these systematic errors could very well be in electronics. Geometry of the setup could be measured and investigated more. As mentioned before, the resolving time can be lowered a bit. But it should not have huge impact on determination of angular correlation coefficients.

8 Acknowledgement

References

[1] Unknown. *Experiment description: Nuclear γ-γ Angular Correlations.* 2019.

[2] Kai Siegbahn, ed. *α-, β-, and γ-Ray Spectroscopy.* Vol. 2. North-Holland Publishing Company, 1965.

[3] E. L. Brady and M. Deutsch. "Angular Correlation of Successive Gamma-Rays". In: *Physical Review* 78.5 (June 1950), pp. 558–566. DOI: 10.1103/PhysRev.78.558.

[4] P.D. Stevenson. "Analytic angular momentum coupling coefficient calculators". In: *Computer Physics Communications* 147.3 (2002), pp. 853–858. ISSN: 0010-4655. DOI: https://doi.org/10.1016/S0010-4655(02)00462-9. URL: http://www.sciencedirect.com/science/article/pii/S0010465502004629.

[5] Plasma Laboratory of Weizmann Institute of Science. *369j-symbol Calculator.* URL: https://plasma-gate.weizmann.ac.il/369j.html.

[6] Robert Allan Wilson. "Directional correlation of the 346-136 keV gamma-gamma cascade in Ta181". MA thesis. Portland State University. Department of Physics, 1969. URL: https://pdxscholar.library.pdx.edu/open_access_etds/75/.

[7] Hermann Kolanoski and Norbert Wermes. *Teilchendetektoren.* Springer Berlin Heidelberg, 2016.

[8] Qwerty123uiop. *File:PhotoMultiplierTubeAndScintillator.svg.* 2013. URL: https://commons.wikimedia.org/wiki/File:PhotoMultiplierTubeAndScintillator.svg.

[9] G. Iaci and M. Lo Savio. "A fast-slow coincidence system". In: *Nuclear Instruments and Methods* 65.1 (1968), pp. 103–109. ISSN: 0029-554X. DOI: https://doi.org/10.1016/0029-554X(68)90014-1. URL: http://www.sciencedirect.com/science/article/pii/0029554X68900141.

[10] Ortec. *Single-Channel Pulse-Height Analyzers.*

[11] Canberra Elektronik. *Constant Fraction Discriminator: Model 1326, 1428* Operating Manual.*

[12] R.B.firestone. *Table of Isotopes.* 8th ed. Wiley, New York, 1996.

[13] Traitor. *File:60Co gamma spectrum energy.png.* 2007. URL: https://en.wikipedia.org/wiki/File:60Co_gamma_spectrum_energy.png.

[14] Adria C. Melissinos and Jim Napolitano. *Experiments in Modern Physics.* Elsevier Science, 2003.